



## OPEN ACCESS

## EDITED BY

Mohammad Islam,  
GE Aviation Systems, United States

## REVIEWED BY

Asif Mahmood,  
The University of Sydney, Australia  
Haris Ansari,  
University of Calgary, Canada

## \*CORRESPONDENCE

Zeeshan Ali,  
zeeshan.ali@scme.nust.edu.pk  
Xiaoming Lin,  
linxm@scnu.edu.cn

## SPECIALTY SECTION

This article was submitted to Energy  
Materials,  
a section of the journal  
Frontiers in Materials

RECEIVED 23 May 2022

ACCEPTED 28 July 2022

PUBLISHED 29 August 2022

## CITATION

Ali Z, Ali M, Mehmood A, Ishfaq A,  
Akram MA, Zeb A and Lin X (2022),  
Nano-architected cobalt selenide  
spheres anchored on graphene oxide  
sheets for sodium ion battery anode.  
*Front. Mater.* 9:950673.  
doi: 10.3389/fmats.2022.950673

## COPYRIGHT

© 2022 Ali, Ali, Mehmood, Ishfaq,  
Akram, Zeb and Lin. This is an open-  
access article distributed under the  
terms of the [Creative Commons  
Attribution License \(CC BY\)](#). The use,  
distribution or reproduction in other  
forums is permitted, provided the  
original author(s) and the copyright  
owner(s) are credited and that the  
original publication in this journal is  
cited, in accordance with accepted  
academic practice. No use, distribution  
or reproduction is permitted which does  
not comply with these terms.

# Nano-architected cobalt selenide spheres anchored on graphene oxide sheets for sodium ion battery anode

Zeeshan Ali<sup>1\*</sup>, Muhammad Ali<sup>1</sup>, Ahtisam Mehmood<sup>1</sup>,  
Ayesha Ishfaq<sup>1</sup>, Muhammad Aftab Akram<sup>1</sup>, Akif Zeb<sup>2</sup> and  
Xiaoming Lin<sup>2\*</sup>

<sup>1</sup>School of Chemical and Materials Engineering (SCME), School of Interdisciplinary Engineering and Sciences (SINES), National University of Sciences and Technology (NUST), Islamabad, Pakistan, <sup>2</sup>School of Chemistry, South China Normal University, Guangzhou, China

Aimed at commercializing the technology of sodium-ion batteries (SIBs), researchers have been trying to produce electrode materials with optimally high charge storage capacity, superior rate capability, extended life, and cost-effective components. Herein, we synthesized an electrode of cobalt selenides loaded in carbon spheres and anchored on reduced graphene (CSSs@rGO) for high-performance SIBs. This improved structure of CSSs@rGO permits the pseudocapacitive storage of charge, thus enhancing the electrical characteristics. It was discovered that the diameter of the carbon sphere had a significant impact on the charge storage capacities of the developed electrode materials, suggesting the probable depth of sodium-ion (Na-ion) movement in the electrode materials during charge and discharge. For instance, CSSs@rGO with an average diameter of ~70 nm presented the best electrochemical performance as an anode of SIBs. The nano-architecture CSSs@rGO exhibits excellent ion storage capability with a reversible capacity of 600 mA h g<sup>-1</sup> at a discharge rate of 100 mA g<sup>-1</sup> after 50 cycles. However, at a higher discharge rate (e.g., 1,000 mA g<sup>-1</sup>), a storage capacity as high as 380 mA h g<sup>-1</sup> was achieved. In addition to higher charge storage capability and efficient charge storage at higher discharge rates, the developed CSSs@rGO exhibited stable cycling performance for over 3,000 cycles, which clearly shows the feasibility of our products. This work will open new approaches for developing advanced electrode materials for high-performance sodium-ion batteries.

## KEYWORDS

cobalt selenide, graphene, sodium-ion batteries, hydrothermal and solvothermal synthesis, nano-architecture

## Introduction

The ubiquitous distribution of sodium metal resources around the world and the low prices of its salts have urged scientists across the globe to consider sodium-ion batteries (SIBs) as a promising alternative to lithium-ion batteries (LIBs) (Slater et al., 2013; Kim et al., 2016; Ali et al., 2020; Rashad et al., 2020; Zhou et al., 2021; Asif et al., 2022). Although the recent studies of SIBs have reported cathode performances comparable to the cathodes of LIBs (Barpanda et al., 2014; Lee et al., 2014; Xiang et al., 2015; Ahsan et al., 2022), the development of an anode with adequately high-energy capacity, sufficiently long cycling life, and applicably low redox potential is still a big challenge for the scientific community. Moreover, the deployment of the already developed LIB anode materials in SIBs has been unsuccessful owing to the greater ionic size and higher molar mass of sodium compared to lithium (Yousaf et al., 2021). Graphite, silicon, and titanium oxide-based materials are effective and mostly used as anodes in LIBs. However, when employed in SIBs, these materials show significant issues (Wang et al., 2013; Wen et al., 2014; Chen et al., 2015; Kim et al., 2015; Asif et al., 2020c). Even an expanded graphite structure can only produce a reversible capacity of  $184 \text{ mA h g}^{-1}$  at  $100 \text{ mA g}^{-1}$  (Wen et al., 2014). “ $\text{P}_2\text{-Na}_{0.66}[\text{Li}_{0.22}\text{Ti}_{0.78}] \text{O}_2$ ,” a layered material, was recently introduced, exhibiting only  $\sim 0.77\%$  volume change during sodium insertion/extraction (Wang et al., 2013; Ali et al., 2020). Although it can exhibit an average storage voltage of  $0.75 \text{ V}$ , it can provide a reversible capacity of only  $116 \text{ mA h g}^{-1}$ . Silicon can concoct a fully sodiated phase NaSi, but the required activation energy is calculated to be higher than  $1 \text{ eV}$ , indicating limited uptake of sodium-ion in pristine silicon. A recent report demonstrated that silicon nano-particles can store sodium ions reversibly and deliver a capacity of  $279 \text{ mA h g}^{-1}$  at a very slow scan rate of  $10 \text{ mA g}^{-1}$  (Xu et al., 2016).

Charge storage mechanisms at the anode could be intercalation, alloying, or conversion. Until now, intercalation-type anode materials such as graphite and  $\text{Na}_3\text{V}_2(\text{PO}_4)_3$  have been mostly used (Cai et al., 2018; Dong et al., 2018; Gu et al., 2018; Yousaf et al., 2021; Zhou et al., 2021). This type presents sufficient cyclic performance and rate capabilities but suffers from low energy capacities (i.e., less than  $300 \text{ mA h g}^{-1}$ ) (Yousaf et al., 2021; Zhou et al., 2021). Materials that store charge by making alloys (e.g., P, Sb, and Ge) or conversion (e.g.,  $\text{SnO}_2$ ,  $\text{MoS}_2$ , and  $\text{NiSe}_2$ ) mechanisms usually possess higher energy capacities but lack longer cycling life due to severe structural deteriorations caused by large volume changes (Dahbi et al., 2016; Jiang et al., 2016; Lu et al., 2017; Luo et al., 2017; Asif et al., 2018; Ahsan et al., 2020). To rectify this problem of structural instability, many authors have successfully presented the incorporation of carbon-based additives to make composite or utilization of 2D structures to compensate for volumetric change materials (Huang et al., 2019; Mahmood et al., 2019; Wang et al., 2019). Transition metal chalcogenides (TMCs) are among these

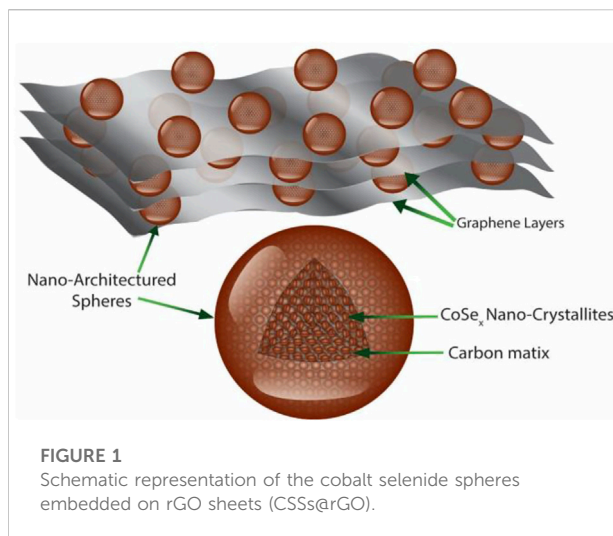


**FIGURE 1**  
Schematic representation of the cobalt selenide spheres embedded on rGO sheets (CSSs@rGO).

conversion mechanism-based anode materials (Ali et al., 2018a; Ali et al., 2018b; Ali et al., 2019; Riaz et al., 2019; Asif et al., 2020b; Mahmood et al., 2020; Rashad et al., 2020; Sajjad et al., 2021; Usman et al., 2022), which have attracted pronounced attraction as anodes of SIBs because of their high theoretical energy capacity, low cost, robust structure, and facile synthesis techniques (Li et al., 2019; Riaz et al., 2019; Ali et al., 2020; Rashad et al., 2020; Wang et al., 2020; Usman et al., 2022). To the best of our knowledge, a spherical structure composed of cobalt selenides in the spherical form embedded on rGO has not been reported yet.

Herein, we present an anode composed of uniquely structured cobalt selenide spheres (CSSs), which are uniformly anchored on reduced graphene oxide (rGO) sheets. These CSSs consist of small crystallites (2–4 nm) of cobalt selenide embedded and dispersed in an amorphous carbon matrix. The carbon matrix not only enhances the electronic properties but also provides the buffers for the volumetric changes during the charge–discharge cycling. CSSs of various diameters (specifically 70, 150, and 300 nm) were produced in this study by controlling the reactant concentrations in a one-step hydrothermal method. Due to their unique structure, CSSs@rGO (with 70 nm diameter spheres) presented extraordinary electrochemical performance as an anode of SIBs. The tapping density of the electrode materials is a big question for the graphene-containing composite electrodes. In our study, tapping density was sufficiently high ( $1.5 \text{ mg cm}^{-2}$ ) as we utilized very small concentrations (2–3wt%) of graphene oxide as the precursor. The composite showed high initial discharge capacity ( $770 \text{ mA h g}^{-1}$  at  $100 \text{ mA g}^{-1}$ ), improved rate capability ( $770 \text{ mA h g}^{-1}$  at  $100 \text{ mA g}^{-1}$  and  $200 \text{ mA h g}^{-1}$  at  $5,000 \text{ mA g}^{-1}$ ), and ultra-long cycle life ( $380 \text{ mA h g}^{-1}$  at  $1,000 \text{ mA g}^{-1}$ ) after 3,000 cycles.

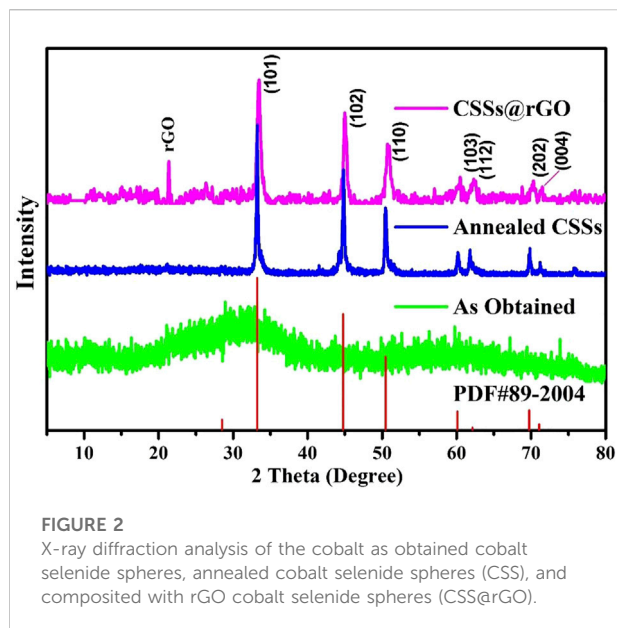


**FIGURE 2**  
X-ray diffraction analysis of the cobalt as obtained cobalt selenide spheres, annealed cobalt selenide spheres (CSS), and composited with rGO cobalt selenide spheres (CSS@rGO).

## Results and discussion

Cobalt selenide spheres were produced by a facile method (for details, see Experiments and methods) where precursors were dissolved in isopropanol in the presence of glycerol and treated hydrothermally. As the CSSs were formed by the well-renowned crystallization and Ostwald growth mechanism, where growth can be controlled by solution viscosity (Meinders and van Vliet, 2004), we utilized varying amounts of glycerol to tailor viscosity. Hence, CSSs with different diameters were produced, and composites with sphere diameters of 70, 150, and 300 nm were termed CSSs70@rGO, CSSs150@rGO, and CSSs300@rGO, respectively. Although the as-obtained spheres were amorphous, crystalline spheres of cobalt selenide were obtained by annealing at 400°C for 3 h. These spheres consist of nano-crystallites embedded in a carbon matrix within the spheres, as illustrated by the schematic in Figure 1.

X-ray diffraction (XRD) analysis was used to investigate the crystalline phases and compositions. Figure 2 shows XRD patterns in a  $2\theta$  range of 5°–80° of the as-obtained, annealed, and anchored on rGO CSSs. The XRD pattern of the as-obtained CSSs does not show the presence of any crystalline phases. However, annealing under optimal conditions (i.e., above recrystallization temperature for a sufficient duration) causes the formation of various crystals. All peaks of the XRD pattern can be attributed to the JCPDS No. 89-2004, indicating the hexagonal symmetry of the CSSs with a space group of P63/mmc. The absence of any other peaks shows good phase purity. Supplementary Figure S1 presents the optimization of annealing conditions for different temperatures and varying durations. XRD peaks become clearer as the annealing temperature is increased from 300°C to 400°C or 500°C. However, the crystalline nature of the CSSs is not affected prominently by longer than 3 h (i.e., 4 or 5 h) annealing durations.

In order to investigate the unique morphologies of the CSSs@rGO composites, scanning electron microscopy (SEM), transmission electron microscopy (TEM), and high-resolution TEM (HRTEM) were employed. The SEM and TEM analyses confirm the uniform distribution and anchoring of CSS over nanosheets of rGO (Figure 3A–D). Moreover, the high-resolution TEM analysis (Figure 3E) of an individual sphere reveals that the cobalt selenide particles are embedded in an amorphous carbon matrix. Furthermore, lattice fringes with a spacing of 0.26 nm agree well with the (101) plane of the hexagonal cobalt selenide (Figure 3E, inset). CSSs of different diameters obtained by varying the glycerol amount are presented in the TEM image (Supplementary Figures S2A–F). CSSs of nearly 700 nm diameters were produced with ~5wt% glycerol, and the diameters decreased by increasing the glycerol amount. To produce CSSs in a nanometer range (<100 nm), the glycerol amount used was 25wt%. A further increase in glycerol amount inhibits the formation of the spherical shape of the particles (Supplementary Figure S2I). SEM images of cobalt selenide spheres prepared with and without rGO solution are presented in Supplementary Figures S3A–C, whereas the CSSs produced without adding rGO are presented in Supplementary Figures S3D–F. Monodispersed sphere-like morphologies are evidenced by the TEM and SEM analyses presented in Supplementary Figures S2G,H, and Supplementary Figure S3, respectively. However, all the CSS spheres seem to be firmly anchored over the rGO sheets.

Elemental mapping of a graphene-embedded cobalt selenide sphere was done using energy dispersive spectroscopy (EDS). Figure 3F confirms the uniform distribution of cobalt, selenium, and carbon across the sphere. Due to the presence of graphene, the carbon signal around the sphere is also high. Hence, composites with cobalt selenide spheres anchored on reduced graphene oxide are ascertained. Such composites are expected to perform extraordinarily as an anode of sodium-ion batteries owing to the enhanced surface area, intimate contact with rGO, and monodispersed nature of chalcogenide species in carbon matrices (Asif et al., 2020a; Maqbool et al., 2020).

The electrochemical performance of the CSSs@rGO was examined by fabricating 2032-type coin cells with sodium metal foil as reference and counter electrode. The literature reveals that ether-based electrolytes yield the best results for TMC-based anodes (Ganesan et al., 2015; Zhang et al., 2015; Zhang et al., 2016a; Zhang et al., 2016b; Ko et al., 2016; Luo et al., 2016; Peng et al., 2016; Su et al., 2016; Zhu et al., 2017). Therefore, an electrolyte containing 1.0 M NaCF<sub>3</sub>SO<sub>3</sub> in an ether-based solvent [diethylene glycol (DEG) and dimethyl ether (DME) in a 1:1 volume ratio] was used in this study. For good cycle stability, the scan voltage window is critical (Xu et al., 2013; Hu et al., 2015; Kim et al., 2015). Thus, varying voltage windows were used in previous reports to optimize the cycling performance. Our initial CV tests revealed that no peaks are present in the voltage range of 0.01–0.5 and 2.5–3.0 V. Hence, learning from CV tests and

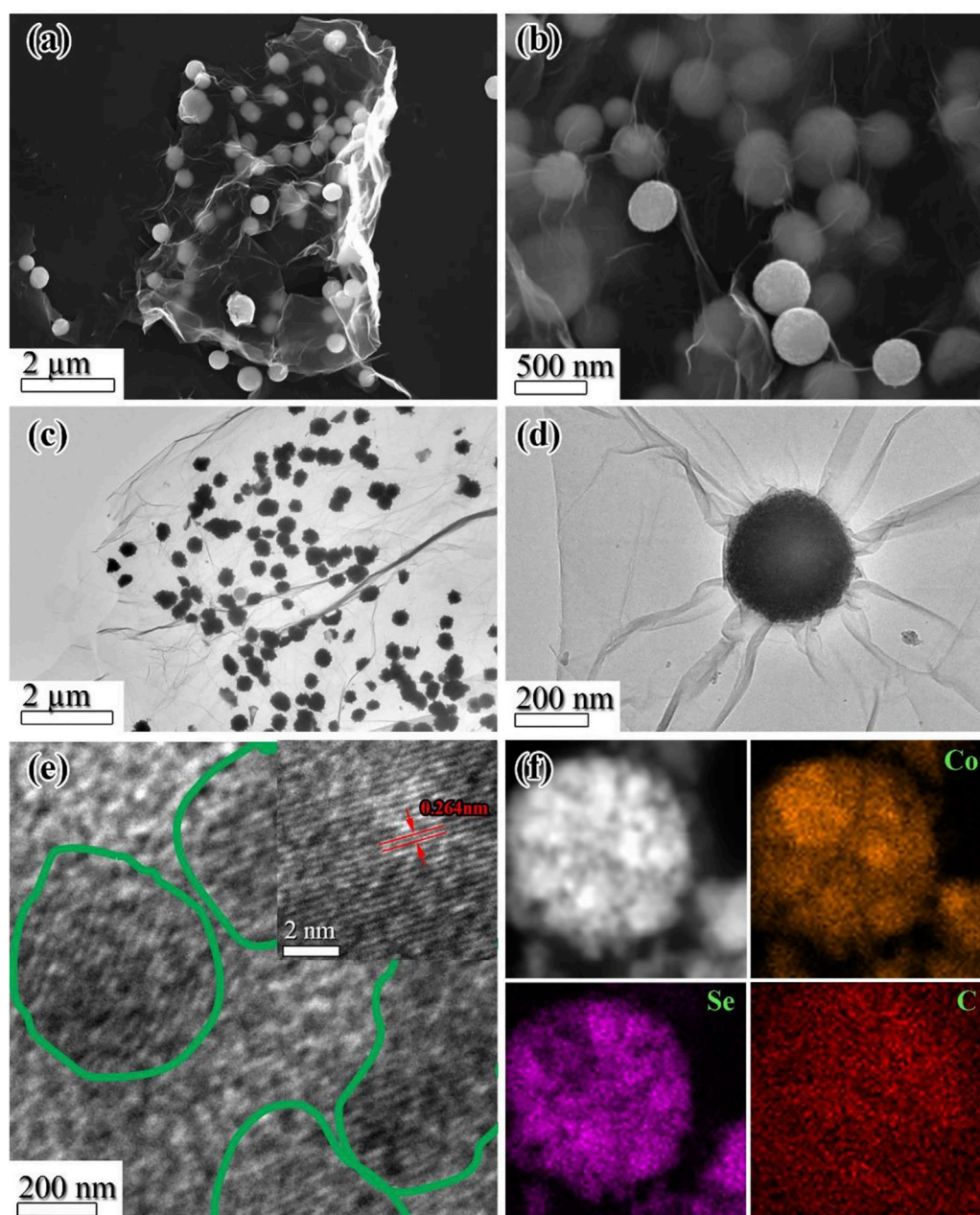


**FIGURE 3**  
 (A,B) SEM images. (C,D) TEM images. (E) High-resolution TEM images. (F) EDS elemental mapping of CSSs@rGO.

previous studies, we have compared the cyclic performance of only two voltage ranges (i.e., 0.1–2.8 and 0.5–2.8 V) at a scan rate of  $2000 \text{ mA g}^{-1}$ . In order to observe a charge–discharge behavior in detail, CV tests were performed for all composites of CSSs@rGO, showing similar behavior to that presented in Figure 4A. In the first cycle, the cathodic peak at 0.95 V can be associated with the solid electrolyte layer (SEI) formation. However, the anodic peaks of 1.75 and 1.81 V can be related to the formation of

$\text{Na}_x\text{CoSe}_2$  and cobalt selenide successively (Tang et al., 2017). From the second cycle onward, the strong cathodic peak at 1.14 V evidences the formation of  $\text{CoSe}_2$  and  $\text{Na}_2\text{Se}$  together, whereas a shallow peak around 0.65 V confirms the formation of Co metal and  $\text{Na}_2\text{Se}$  (Cui et al., 2018). Meanwhile, the anodic peak of 1.81 V confirms the reformation of cobalt selenide from  $\text{Na}_2\text{Se}$ . The charge–discharge behavior for the 1st and 10th cycles (Figure 4C) is consistent with the CV data, proving the

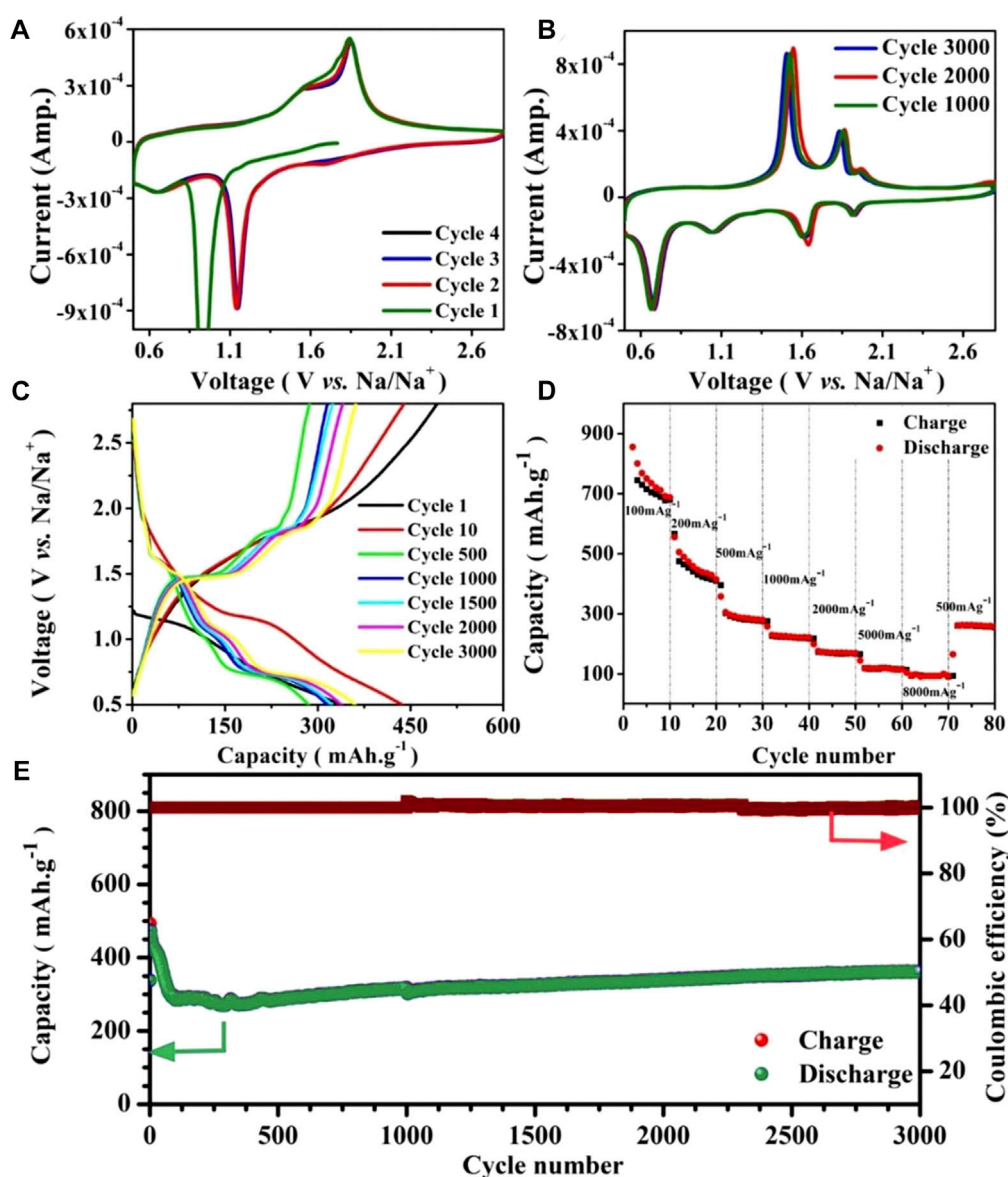


FIGURE 4

Electrochemical performance of CSSs70@rGO, (A) CV curves of as-prepared, and (B) cycled cells at the scan rate of  $1 \text{ mV s}^{-1}$  between 0.5 and 2.8 V. (C) Charge–discharge curves at  $1,000 \text{ mA g}^{-1}$  scan rate. (D) Rate performance of CSSs70@rGO. (E) Long-term cyclic performance of CSSs70@rGO at the scan rate of  $1,000 \text{ mA g}^{-1}$ .

validity of these findings. Reversible Na-ion storage causes changes in the morphology and electrochemical activity of electrode materials, increasing the charge storage capacity (Zhang et al., 2015; Zhang et al., 2016a; Liu et al., 2016). However, the formation of unstable SEI or phase changes (activation) of material structure may reduce the charge storage capacity (Ge et al., 2018). Reports on cobalt selenide have described both the descent and increase in capacity as a result of these competing mechanisms (Zhang et al., 2015; Zhang et al., 2016a; Liu et al., 2016; Ge et al., 2018). We observed a steady

drop in the charge storage capacity of CSSs@rGO throughout the first 70 cycles until it reached a steady level. During these cycles, a discharge plateau at 1.14 V and a charge plateau at 1.82 V are shown in charge–discharge curves (Figure 4C), consistent with the CV results of Figure 4A. The charge–discharge patterns undergo a significant reorganization throughout the subsequent cycles. After the activation (rearrangement), the (dis)charge patterns become stable. Subsequently, the material shows extraordinary stability even after 3,000 cycles. Similar activation behavior was reported and described in the

literature because of the morphological or phase changes in electrode materials (Zhang et al., 2016a; Ali et al., 2018b; Ge et al., 2018). After the activation process, CV tests were conducted at 1,000, 2,000, and 3,000 cycles (Figure 4B), showing overlapping patterns indicating the materials' persistent electrochemical activity. These CV scans contain four cathodic peaks: 1.83 V for Na-ion adsorption, 1.69 V for the formation of  $\text{Na}_x\text{CoSe}_2$  intermediate phase, 1.14 V for the generation reaction of  $\text{CoSe}_2$  and  $\text{Na}_2\text{Se}$ , and around 0.65 V confirming the formation of Co metal and  $\text{Na}_2\text{Se}$ . Each of these CV scans depicted two anodic peaks (centered at 1.5 and 1.9 V) corresponding to the regeneration of Na ions from the  $\text{Na}_x\text{CoSe}_2$  intermediate phase and  $\text{Na}_2\text{Se}$ , respectively (Tang et al., 2017; Cui et al., 2018). These CV curves were consistent with discharge-charge curves shown in Figure 4C.

The performance rate of the CSSs70@rGO is presented in Figure 4D. As the current densities gradually increase from 100 to 200, 500, 1,000, and 2,000  $\text{mA g}^{-1}$ , the discharge capacities change from 855 to 555, 358, 258, and 200  $\text{mA h g}^{-1}$ , respectively. Even at ultrahigh current densities of 5,000 and 10,000  $\text{mA g}^{-1}$ , the discharge capacities remain 144 and 105  $\text{mA h g}^{-1}$ , respectively. Moreover, when the current density is reduced back to 500  $\text{mA g}^{-1}$ , the capacity can recover to 263  $\text{mA h g}^{-1}$ . This outstanding rate capability could arise from the intimate contact between crystallites of cobalt selenide and carbon matrix, which helps in faster ion/charge transfer at higher scan rates.

The long-term cycling performance of the CSSs70@rGO at a current rate of 1,000  $\text{mA g}^{-1}$  is presented in Figure 4E. The energy capacity becomes stable after about 80 cycles, and the capacity values can reach 350  $\text{mA h g}^{-1}$  even after 3,000 cycles at a scan rate of 1,000  $\text{mA g}^{-1}$ , which is 110 % and 72% of those at the 80th and 5th cycles, respectively. Specific capacity increases after 500 cycles because  $\text{Na}^+$  ions could diffuse to the outer reduced graphene oxide before they get to the active material. Therefore, the  $\text{Na}^+$  ions may diffuse into the CSS *via* vacancies or defects present in the reduced graphene oxide instead of the intercalation mechanism (Yousaf et al., 2019). The coulombic efficiency always ranges between 99.66 % and 102.21% for all the cycles, except for the first cycle.

Such outstanding electrochemical properties and extraordinary cyclability (380  $\text{mA h g}^{-1}$  even after 3,000 cycles at 1  $\text{A g}^{-1}$ ) render the CSSs@rGO as a potential anode material for SIBs. These unparalleled properties can be attributed to some reasons. First, carbon matrix existence in material improves the electronic conductivity and provides the buffer for volumetric changes during intercalation/deintercalation of ions. Second, for the redox processes, the major portion of charge storage is pseudocapacitive behaviors. The last but most important reason is the intimate contact between crystallites of cobalt selenide and the carbon matrix of miniaturized spheres, which makes a smooth transfer of charges during repeated cycles and eases off the kinetic impedance associated with the transport of ions through the material.

## Conclusion

In summary, the monodispersed spheres of cobalt selenide embedded on rGO (CSSs@rGO) were produced *via* a one-step hydrothermal process. Controllable, different sizes of spheres were synthesized by varying reactant concentrations. As an anode of SIBs, the CSSs@rGO presented an extraordinarily reversible specific capacity of 390  $\text{mA h g}^{-1}$  even after 3,000 cycles at the scan rate of 1,000  $\text{mA g}^{-1}$ . At a slow scan rate such as 100  $\text{mA g}^{-1}$ , the specific capacity was as high as 554  $\text{mA h g}^{-1}$  after 50 cycles. This outstanding cycling performance can be attributed to the intimate contact between crystallites of cobalt selenide and the carbon matrix of nanospheres. Moreover, the pseudocapacitive behaviors in the redox reaction also take part in enhancing rate capability and cyclability. Such intriguing electrochemical properties render CSSs@rGO a potential material for SIBs anode.

## Experiments and methods

### Synthesis of CSSs and CSS@rGO

CSSs were produced *via* a facile single-step hydrothermal process. In a typical synthesis; 0.3 mol of  $\text{Co}(\text{NO}_3)_2 \cdot 6\text{H}_2\text{O}$  (cobalt nitrate hexahydrate) and 0.1 mol of  $\text{H}_3\text{O}_2\text{Se}$  (selenous acid) were dissolved in 40 ml of  $(\text{CH}_3)_2\text{CHOH}$  (isopropanol) + 20% glycerol, by magnetic stirring at 40°C for half an hour to obtain a dark purple solution, to which a separately prepared 5 ml rGO/isopropanol solution of 1  $\text{mg ml}^{-1}$  was added. This solution was transferred to a Teflon-lined stainless-steel container and treated hydrothermally for 6 hours at 120°C–150°C. After natural cooling to room temperature, the product was centrifuged and washed thoroughly with absolute ethanol several times. As-obtained purple precipitates were dried at 70°C for 12 h under vacuum conditions. The product was then annealed at 400°C under a nitrogen environment for 5 h with a heating rate of 5°C per min. Then, reduced graphene oxide sheets were mixed with annealed material in absolute ethanol and sonicated for 1 h to obtain  $\text{CoSe}_2$ @GO composite.

### Material characterization

X-ray diffraction (XRD) studies were done using a PAN analytical X'Pert-3 Powder X-ray diffractometer equipped with Cu K $\alpha$  radiation. The accelerating voltage and current were 40 kV and 40 mA, respectively. The XRD analysis was performed in the  $2\theta$  range of 5°–80°. The morphological characterization of the product was carried out using FEI Tecnai T20, F20, and F30 transmission electron microscopes. The elemental composition of composites was analyzed by an energy dispersive spectroscopy detector equipped with F30 and

X-ray photoelectron spectroscopy (XPS), Kratos Axis Ultra with monochromatized Al K $\alpha$  radiation (1,486.6 eV). The BET analysis was done using ASAP 2010. The thermogravimetric analysis (TGA) was carried out by an SDT Q600 (USA) in argon at a heating rate of 5°C per min from 25°C to 900°C.

## Electrochemical analysis

The working electrode was prepared by mixing the active materials (CSSs or CSSs@rGO), conductive agent (acetylene black), and binder (carboxymethylcellulose sodium) in a weight ratio of 80:10:10, respectively. A homogenous slurry (obtained by mixing in deionized water) was then pasted onto a well-cleaned Cu foil and dried at 70°C for 24 h under a vacuum. The final mass loading of active material was between 1.00 and 1.2 mg cm<sup>-2</sup>. Na foil cut into circular disks was used as reference and counter electrodes. A glass fiber filter paper was used as a separator. The 2032-type coin half cells were fabricated in an Ar-filled glovebox. The electrolyte was 1 mol dm<sup>-3</sup> of sodium trifluoro-methane-sulfonate (NaCF<sub>3</sub>SO<sub>3</sub>) in an ether-based solvent (diethylene glycol (DEG) and dimethyl ether (DME) in 1:1 volume ratio). Electrochemical measurements of the prepared half cells were carried out with a LAND CT 2001A analyzer at different current densities with a potential window of 0.1–2.8 V vs. Na<sup>+</sup>/Na. Cyclic Voltammetry tests were performed in the same voltage range, and electrochemical impedance spectroscopy (EIS) was carried out in the frequency range of 100 kHz to 100 mHz with a sinusoidal voltage signal of 5 mV using CHI 760C equipment (Shanghai Chenhua).

## Data availability statement

The original contributions presented in the study are included in the article/Supplementary Material. Further inquiries can be directed to the corresponding author.

## References

- Ahsan, M. T., Ali, Z., Usman, M., and Hou, Y. (2022). Unfolding the structural features of NASICON materials for sodium-ion full cells. *Carbon Energy*, 1–44. doi:10.1002/cey2.222/cey2.222
- Ahsan, M. T., Usman, M., Ali, Z., Javed, S., Ali, R., Farooq, M. U., et al. (2020). 3D hierarchically mesoporous zinc-nickel-cobalt ternary oxide (Zn<sub>0.6</sub>Ni<sub>0.8</sub>Co<sub>1.6</sub>O<sub>4</sub>) nanowires for high-performance asymmetric supercapacitors. *Front. Chem.* 8 (487). doi:10.3389/fchem.2020.00487
- Ali, Z., Asif, M., Huang, X., Tang, T., and Hou, Y. (2018a). Hierarchically porous Fe<sub>2</sub>CoSe<sub>4</sub> binary-metal selenide for extraordinary rate performance and durable anode of sodium-ion batteries. *Adv. Mat.* 30 (32), 1802745. doi:10.1002/adma.201802745
- Ali, Z., Asif, M., Zhang, T., Huang, X., and Hou, Y. (2019). General approach to produce nanostructured binary transition metal selenides as high-performance sodium ion battery anodes. *Small* 15 (33), 1901995. doi:10.1002/smll.201901995

## Author contributions

The manuscript was written with the contributions of all authors. All authors have given approval to the final version of the manuscript.

## Funding

This work was supported by the seed funding scheme of the National University of Sciences and Technology (NUST), H-12, Islamabad, and Pakistan Science Foundation Grant PSF-NSFC-IV/Eng/C-NUST (22).

## Conflict of interest

The authors declare that the research was conducted in the absence of any commercial or financial relationships that could be construed as a potential conflict of interest.

## Publisher's note

All claims expressed in this article are solely those of the authors and do not necessarily represent those of their affiliated organizations or those of the publisher, the editors, and the reviewers. Any product that may be evaluated in this article, or claim that may be made by its manufacturer, is not guaranteed or endorsed by the publisher.

## Supplementary material

The Supplementary Material for this article can be found online at: <https://www.frontiersin.org/articles/10.3389/fmats.2022.950673/full#supplementary-material>

- Ali, Z., Tang, T., Huang, X., Wang, Y., Asif, M., and Hou, Y. (2018b). Cobalt selenide decorated carbon spheres for excellent cycling performance of sodium ion batteries. *Energy Storage Mater.* 13, 19–28. doi:10.1016/j.ensm.2017.12.014
- Ali, Z., Zhang, T., Asif, M., Zhao, L., Yu, Y., and Hou, Y. (2020). Transition metal chalcogenide anodes for sodium storage. *Mater. Today* 35, 131–167. doi:10.1016/j.mattod.2019.11.008
- Asif, M., Ali, Z., Ali, M., and Rashad, M. (2022). Investigating role of ammonia in nitrogen-doping and suppressing polyselenide shuttle effect in Na-Se batteries. *J. Colloid Interface Sci.* 617, 641–650. doi:10.1016/j.jcis.2022.03.024
- Asif, M., Ali, Z., Qiu, H., Rashad, M., and Hou, Y. (2020a). Confined polysulfide shuttle by nickel disulfide nanoparticles encapsulated in graphene nanoshells synthesized by cooking oil. *ACS Appl. Energy Mat.* 3 (4), 3541–3552. doi:10.1021/acsaem.0c00072
- Asif, M., Rashad, M., Ali, Z., and Ahmed, I. (2020c). Synthesis of ternary metal oxides as positive electrodes for Mg–Li hybrid ion batteries. *Nanoscale* 12 (2), 924–932. doi:10.1039/C9NR08758C

- Asif, M., Rashad, M., and Ali, Z. (2020b). Electrochemical intercalations of divalent ions inside Ni/Zn co-doped cobalt sulfide nanoparticle decorated carbon spheres with superior capacity. *Nanoscale* 12 (26), 14267–14278. doi:10.1039/D0NR02761H
- Asif, M., Rashad, M., Ali, Z., Qiu, H., Li, W., Pan, L., et al. (2018). Ni-doped MnO<sub>2</sub>/CNT nanoarchitectures as a cathode material for ultra-long life magnesium/lithium hybrid ion batteries. *Mater. Today Energy* 10, 108–117. doi:10.1016/j.mtener.2018.08.010
- Barpanda, P., Oyama, G., Nishimura, S.-i., Chung, S.-C., and Yamada, A. (2014). A 3.8-V earth-abundant sodium battery electrode. *Nat. Commun.* 5, 4358. doi:10.1038/ncomms5358
- Cai, Y. S., Cao, X. X., Luo, Z. G., Fang, G. Z., Liu, F., Zhou, J., et al. (2018). Caging Na<sub>3</sub>V<sub>2</sub>(PO<sub>4</sub>)<sub>2</sub>F-3 microcubes in cross-linked graphene enabling ultrafast sodium storage and long-term cycling. *Adv. Sci. (Weinh)* 5 (9), 1800680. doi:10.1002/advs.201800680
- Chen, Y., Liu, L., Xiong, J., Yang, T., Qin, Y., and Yan, C. (2015). Porous Si nanowires from cheap metallurgical silicon stabilized by a surface oxide layer for lithium ion batteries. *Adv. Funct. Mat.* 25 (43), 6701–6709. doi:10.1002/adfm.201503206
- Cui, C., Wei, Z. X., Zhou, G., Wei, W. F., Ma, J. M., Chen, L. B., et al. (2018). Quasi-reversible conversion reaction of CoSe<sub>2</sub>/nitrogen-doped carbon nanofibers towards long-lifetime anode materials for sodium-ion batteries. *J. Mat. Chem. A Mat.* 6 (16), 7088–7098. doi:10.1039/c8ta01168k
- Dahbi, M., Yabuuchi, N., Fukunishi, M., Kubota, K., Chihara, K., Tokiwa, K., et al. (2016). Black phosphorus as a high-capacity, high-capability negative electrode for sodium-ion batteries: Investigation of the electrode/electrolyte interface. *Chem. Mat.* 28 (6), 1625–1635. doi:10.1021/acs.chemmater.5b03524
- Dong, B., Ju, Y., Huang, X., Li, W., Ali, Z., Yin, H., et al. (2018). A general strategy for facile synthesis of ultrathin transition metal hydroxide nanosheets. *Nanoscale* 11 (12), 5141–5144. doi:10.1039/C8NR04922F
- Ganesan, P., Prabu, M., Sanetuntikul, J., and Shanmugam, S. (2015). Cobalt sulfide nanoparticles grown on nitrogen and sulfur codoped graphene oxide: An efficient electrocatalyst for oxygen reduction and evolution reactions. *ACS Catal.* 5 (6), 3625–3637. doi:10.1021/acscatal.5b00154
- Ge, P., Hou, H. S., Li, S. J., Huang, L. P., and Ji, X. B. (2018). Three-dimensional hierarchical framework assembled by cobblestone-like CoSe<sub>2</sub>@C nanospheres for ultrastable sodium-ion storage. *ACS Appl. Mat. Interfaces* 10 (17), 14716–14726. doi:10.1021/acsami.8b01888
- Gu, E. L., Liu, S. H., Zhang, Z. Z., Fang, Y. Y., Zhou, X. S., and Bao, J. C. (2018). An efficient sodium-ion battery consisting of reduced graphene oxide bonded Na<sub>3</sub>V<sub>2</sub>(PO<sub>4</sub>)<sub>3</sub> in a composite carbon network. *J. Alloys Compd.* 767, 131–140. doi:10.1016/j.jallcom.2018.07.082
- Hu, Z., Zhu, Z., Cheng, F., Zhang, K., Wang, J., Chen, C., et al. (2015). Pyrite FeS<sub>2</sub> for high-rate and long-life rechargeable sodium batteries. *Energy Environ. Sci.* 8 (4), 1309–1316. doi:10.1039/C4EE03759F
- Huang, X., Shen, T., Zhang, T., Qiu, H., Gu, X., Ali, Z., et al. (2019). Efficient oxygen reduction catalysts of porous carbon nanostructures decorated with transition metal species. *Adv. Energy Mat.* 10 (11), 1900375. doi:10.1002/aenm.201900375
- Jiang, Q., Xu, L., Chen, N., Zhang, H., Dai, L., and Wang, S. (2016). Facile synthesis of black phosphorus: An efficient electrocatalyst for the oxygen evolving reaction. *Angew. Chem. Int. Ed.* 55 (44), 13849–13853. doi:10.1002/anie.201607393
- Kim, H., Hong, J., Park, Y.-U., Kim, J., Hwang, I., and Kang, K. (2015). Sodium storage behavior in natural graphite using ether-based electrolyte systems. *Adv. Funct. Mat.* 25 (4), 534–541. doi:10.1002/adfm.201402984
- Kim, H., Kim, H., Ding, Z., Lee, M. H., Lim, K., Yoon, G., et al. (2016). Recent progress in electrode materials for sodium-ion batteries. *Adv. Energy Mat.* 6 (19), 1600943–n/a. doi:10.1002/aenm.201600943
- Ko, Y. N., Choi, S. H., and Kang, Y. C. (2016). Hollow cobalt selenide microspheres: Synthesis and application as anode materials for Na-ion batteries. *ACS Appl. Mat. Interfaces* 8 (10), 6449–6456. doi:10.1021/acsami.5b11963
- Lee, H.-W., Wang, R. Y., Pasta, M., Woo Lee, S., Liu, N., and Cui, Y. (2014). Manganese hexacyanomanganate open framework as a high-capacity positive electrode material for sodium-ion batteries. *Nat. Commun.* 5, 5280. doi:10.1038/ncomms6280
- Li, Y., Wang, Z., Ali, Z., Tian, K., Xu, J., Li, W., et al. (2019). Monodisperse Fe<sub>3</sub>O<sub>4</sub> spheres: Large-scale controlled synthesis in the absence of surfactants and chemical kinetic process. *Sci. China Mat.* 62 (10), 1488–1495. doi:10.1007/s40843-019-9466-x
- Liu, X., Zhang, K., Lei, K., Li, F., Tao, Z., and Chen, J. (2016). Facile synthesis and electrochemical sodium storage of CoS<sub>2</sub> micro/nano-structures. *Nano Res.* 9 (1), 198–206. doi:10.1007/s12274-016-0981-5
- Lu, Y. Y., Zhang, N., Jiang, S., Zhang, Y. D., Zhou, M., Tao, Z. L., et al. (2017). High-capacity and ultrafast Na-ion storage of a self-supported 3D porous antimony persulfide-graphene foam architecture. *Nano Lett.* 17 (6), 3668–3674. doi:10.1021/acs.nanolett.7b00889
- Luo, W., Calas, A., Tang, C., Li, F., Zhou, L., and Mai, L. (2016). Ultralong Sb<sub>2</sub>Se<sub>3</sub> nanowire-based free-standing membrane anode for lithium/sodium ion batteries. *ACS Appl. Mat. Interfaces* 8 (51), 35219–35226. doi:10.1021/acsami.6b11544
- Luo, W., Gaumet, J.-J., and Mai, L.-Q. (2017). Antimony-based intermetallic compounds for lithium-ion and sodium-ion batteries: Synthesis, construction and application. *Rare Met.* 36 (5), 321–338. doi:10.1007/s12598-017-0899-4
- Mahmood, A., Ali, Z., Tabassum, H., Akram, A., Aftab, W., Ali, R., et al. (2020). Carbon fibers embedded with iron selenide (Fe<sub>3</sub>Se<sub>4</sub>) as anode for high-performance sodium and potassium ion batteries. *Front. Chem.* 8 (408), 408. doi:10.3389/fchem.2020.00408
- Mahmood, A., Li, S., Ali, Z., Tabassum, H., Zhu, B., Liang, Z., et al. (2019). Ultrafast sodium/potassium-ion intercalation into hierarchically porous thin carbon shells. *Adv. Mat.* 31 (2), 1805430. doi:10.1002/adma.201805430
- Maqbool, M., Guo, H., Bashir, A., Usman, A., Abid, A. Y., He, G., et al. (2020). Enhancing through-plane thermal conductivity of fluoropolymer composite by developing *in situ* nano-urethane linkage at graphene–Graphene interface. *Nano Res.* 13, 2741–2748. doi:10.1007/s12274-020-2921-7
- Meinders, M. B. J., and van Vliet, T. (2004). The role of interfacial rheological properties on Ostwald ripening in emulsions. *Adv. Colloid Interface Sci.* 108–109, 119–126. doi:10.1016/j.cis.2003.10.005
- Peng, S., Han, X., Li, L., Zhu, Z., Cheng, F., Srinivansan, M., et al. (2016). Unique cobalt sulfide/reduced graphene oxide composite as an anode for sodium-ion batteries with superior rate capability and long cycling stability. *Small* 12 (10), 1359–1368. doi:10.1002/sml.201502788
- Rashad, M., Asif, M., and Ali, Z. (2020). Quest for magnesium-sulfur batteries: Current challenges in electrolytes and cathode materials developments. *Coord. Chem. Rev.* 415, 213312. doi:10.1016/j.ccr.2020.213312
- Riaz, M. S., Yuan, X., Zhao, Y., Dong, C., Nong, S., Ali, Z., et al. (2019). Porous NiCo<sub>2</sub>S<sub>4</sub>/Co<sub>9</sub>S<sub>8</sub> microcubes templated by sacrificial ZnO spheres as an efficient bifunctional oxygen electrocatalyst. *Adv. Sustain. Syst.* 3 (5), 1800167. doi:10.1002/adsu.201800167
- Sajjad, A., Bhatti, S. H., Ali, Z., Jaffari, G. H., Khan, N. A., Rizvi, Z. F., et al. (2021). Photoinduced fabrication of zinc oxide nanoparticles: Transformation of morphological and biological response on light irradiance. *ACS Omega* 6 (17), 11783–11793. doi:10.1021/acsomega.1c01512
- Slater, M. D., Kim, D., Lee, E., and Johnson, C. S. (2013). Sodium-ion batteries. *Adv. Funct. Mat.* 23 (8), 947–958. doi:10.1002/adfm.201200691
- Su, D., Kretschmer, K., and Wang, G. (2016). Improved electrochemical performance of Na-ion batteries in ether-based electrolytes: A case study of ZnS nanospheres. *Adv. Energy Mat.* 6 (2), 1501785–n. doi:10.1002/aenm.201501785
- Tang, Y., Zhao, Z., Hao, X., Wang, Y., Liu, Y., Hou, Y., et al. (2017). Engineering hollow polyhedrons structured from carbon-coated CoSe<sub>2</sub> nanospheres bridged by CNTs with boosted sodium storage performance. *J. Mat. Chem. A Mat.* 5 (26), 13591–13600. doi:10.1039/C7TA02665J
- Usman, M., Ahsan, M. T., Javed, S., Ali, Z., Zhan, Y., Ahmed, I., et al. (2022). Facile synthesis of iron nickel cobalt ternary oxide (FNCO) mesoporous nanowires as electrode material for supercapacitor application. *J. Materiomics* 8, 221–228. doi:10.1016/j.jmat.2021.03.012
- Wang, Y., Li, M., Xu, L., Tang, T., Ali, Z., Huang, X., et al. (2019). Polar and conductive iron carbide@N-doped porous carbon nanosheets as a sulfur host for high performance lithium sulfur batteries. *Chem. Eng. J.* 358, 962–968. doi:10.1016/j.cej.2018.10.086
- Wang, Y. S., Yu, X. Q., Xu, S. Y., Bai, J. M., Xiao, R. J., Hu, Y. S., et al. (2013). A zero-strain layered metal oxide as the negative electrode for long-life sodium-ion batteries. *Nat. Commun.* 4, 2365. doi:10.1038/ncomms3365
- Wang, Z., Li, Z., Sun, Z., Wang, S., Ali, Z., Zhu, S., et al. (2020). Visualization nanozyme based on tumor microenvironment “unlocking” for intensive combination therapy of breast cancer. *Sci. Adv.* 6 (48), eabc8733. doi:10.1126/sciadv.abc8733
- Wen, Y., He, K., Zhu, Y., Han, F., Xu, Y., Matsuda, I., et al. (2014). Expanded graphite as superior anode for sodium-ion batteries. *Nat. Commun.* 5, 4033. doi:10.1038/ncomms5033

- Xiang, X., Zhang, K., and Chen, J. (2015). Recent advances and prospects of cathode materials for sodium-ion batteries. *Adv. Mat.* 27 (36), 5343–5364. doi:10.1002/adma.201501527
- Xu, Y., Swaans, E., Basak, S., Zandbergen, H. W., Borsa, D. M., and Mulder, F. M. (2016). Reversible Na-ion uptake in Si nanoparticles. *Adv. Energy Mat.* 6 (2), 1501436–n/a. doi:10.1002/aenm.201501436
- Xu, Y., Zhu, Y., Liu, Y., and Wang, C. (2013). Electrochemical performance of porous carbon/tin composite anodes for sodium-ion and lithium-ion batteries. *Adv. Energy Mat.* 3 (1), 128–133. doi:10.1002/aenm.201200346
- Yousaf, M., Naseer, U., Li, Y., Ali, Z., Mahmood, N., Wang, L., et al. (2021). A mechanistic study of electrode materials for rechargeable batteries beyond lithium ions by *in situ* transmission electron microscopy. *Energy Environ. Sci.* 14 (5), 2670–2707. doi:10.1039/d0ee03295f
- Yousaf, M., Wang, Y., Chen, Y., Wang, Z., Firdous, A., Ali, Z., et al. (2019). A 3D trilayered CNT/MoSe<sub>2</sub>/C heterostructure with an expanded MoSe<sub>2</sub> interlayer spacing for an efficient sodium storage. *Adv. Energy Mat.* 9 (30), 1900567. doi:10.1002/aenm.201900567
- Zhang, K., Hu, Z., Liu, X., Tao, Z., and Chen, J. (2015). FeSe<sub>2</sub> microspheres as a high-performance anode material for Na-ion batteries. *Adv. Mat.* 27 (21), 3305–3309. doi:10.1002/adma.201500196
- Zhang, K., Park, M., Zhou, L., Lee, G.-H., Li, W., Kang, Y.-M., et al. (2016). Urchin-like CoSe<sub>2</sub> as a high-performance anode material for sodium-ion batteries. *Adv. Funct. Mat.* 26, 6728–6735. doi:10.1002/adfm.201602608
- Zhang, K., Park, M., Zhou, L., Lee, G.-H., Shin, J., Hu, Z., et al. (2016b). Cobalt-Doped FeS<sub>2</sub> nanospheres with complete solid solubility as a high-performance anode material for sodium-ion batteries. *Angew. Chem. Int. Ed.* 55 (41), 12822–12826. doi:10.1002/anie.201607469
- Zhou, J., Zeng, C., Ou, H., Yang, Q., Xie, Q., Zeb, A., et al. (2021). Metal-organic framework-based materials for full cell systems: A review. *J. Mat. Chem. C Mat.* 9 (34), 11030–11058. doi:10.1039/d1tc01905h
- Zhu, S., Li, Q., Wei, Q., Sun, R., Liu, X., An, Q., et al. (2017). NiSe<sub>2</sub> nanooctahedra as an anode material for high-rate and long-life sodium-ion battery. *ACS Appl. Mat. Interfaces* 9 (1), 311–316. doi:10.1021/acsami.6b10143